ACS Energy LETTERS

http://pubs.acs.org/journal/aelccp

LETTER

Effect of Antisolvent Additives in Aqueous Zinc Sulfate Electrolytes for Zinc Metal Anodes: The Case of Acetonitrile

Stefan Ilic, Michael J. Counihan, Sydney N. Lavan, Yingjie Yang, Yinke Jiang, Diwash Dhakal, Julian Mars, Emma N. Antonio, Luis Kitsu Iglesias, Timothy T. Fister, Yong Zhang, Edward J. Maginn, Michael F. Toney, Robert F. Klie, Justin G. Connell, and Sanja Tepavcevic*

Cite This: *ACS Energy Lett.* 2024, 9, 201−208

Read Online

ACCESS | Metrics & More | Article Recommendations | Supporting Information

ABSTRACT: **Aqueous zinc-ion batteries (ZIBs) employing zinc metal anodes are gaining traction as batteries for moderate to long duration energy storage at scale. However, corrosion of the zinc metal anode through reaction with water limits battery efficiency. Much research in the past few years has focused on additives that decrease hydrogen evolution, but the precise mechanisms by which this takes place are often understudied and remain unclear. In this work, we study the role of an acetonitrile antisolvent additive in improving the performance of aqueous $ZnSO_4$ electrolytes using experimental and computational techniques. We demonstrate that acetonitrile actively modifies the interfacial chemistry during Zn metal plating, which results in improved performance of acetonitrile-containing electrolytes. Collectively, this work demonstrates the effectiveness of solvent additive systems in battery performance and durability and provides a new framework for future efforts to optimize ion transport and performance in ZIBs.**

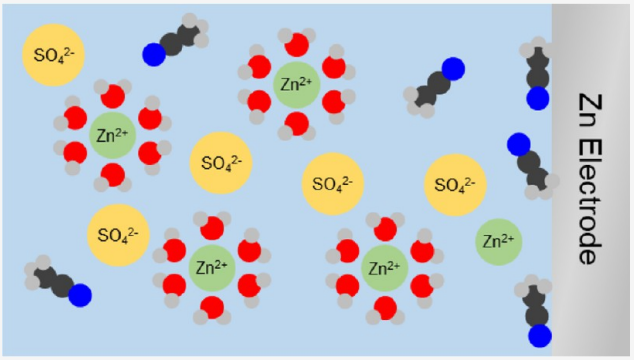

With the ever-growing energy demands, it is of utmost importance to develop efficient and clean energy storage systems.[1] The development of lithium-ion batteries (LIBs) has enabled a wide range of energy storage applications and shaped modern electronic technologies, with the discoveries of portable electronic devices and electric vehicles being among the most widely recognized. Despite the successes of LIBs, advances in technologies for long duration renewable energy storage will require batteries with longer lifetimes, inexpensive and stable supply chains, and improved safety. Aqueous zinc-ion batteries (ZIBs) employing zinc metal anodes are emerging as promising candidates for such applications due the abundance of zinc resources, the lower costs and improved safety of aqueous systems, and the potential for longer lifespans relative to LIBs.[2−4] However, several outstanding challenges need to be addressed before widespread adoption of ZIBs is realized. One of the main challenges is associated with unwanted processes that take place at the electrolyte−metal interface. In particular, aqueous ZIBs employing zinc metal anodes suffer from parasitic hydrogen evolution reaction (HER) at near-neutral pH, which lowers the Coulombic efficiency (CE) and often leads to irreversible Zn corrosion, e.g., via formation of $Zn_4(OH)_6SO_4$ (zinc hydroxysulfate, ZHS) in sulfate-based electrolytes. It is important to note that the presence of ZHS is beneficial for Zn-ion transport, as several reports showed improvements in the ionic conductivities in ZHS layers.[5,6] However, ZHS formation occurs continuously and leads to the complete depletion of active Zn^{2+} over time, unlike in Li systems where the SEI formation prevents further passivation.

A great deal of scientific effort has been aimed at addressing these challenges, and several strategies have been proposed.[5−15] Addition of a high molality of supporting salts has been demonstrated as highly effective in suppressing H_2O activity. Also known as water-in-salt electrolytes (WiSE),[7] this strategy has been initially demonstrated using lithium bis(trifluoromethanesulfonyl)imide, where >20 *m* of the supporting electrolyte effectively reduces the concentration of free

Received: November 20, 2023
Accepted: December 1, 2023
Published: December 20, 2023

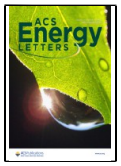

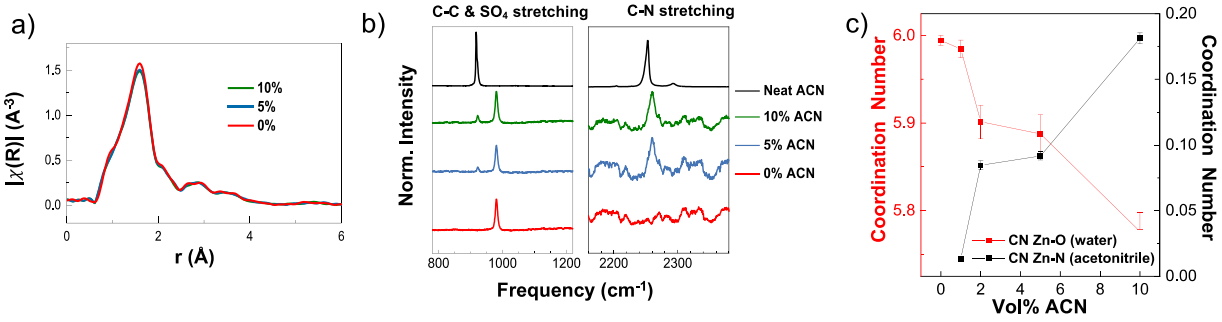

Figure 1. Effect of acetonitrile on the solvation of Zn^{2+} in the bulk electrolyte: (a) EXAFS of 1 M $ZnSO_4$ with varying concentrations of acetonitrile; (b) Raman spectra of different bands for 1 M $ZnSO_4$ electrolytes with varying concentrations of acetonitrile; and (c) calculated coordination numbers for Zn−O with water and Zn−N with acetonitrile in samples with up to 10% acetonitrile.

water and displaces water molecules at the metal−electrolyte interface, lowering the rate of HER. Since then, the WiSE strategy has been successfully applied to other electrolyte mixtures.[8−10] Nevertheless, improvements in the electrochemical activity of WiSEs are still overshadowed by the high cost and high viscosity of these electrolytes.[11] Another effective strategy involves the use of organic additives that have higher Gutmann donor numbers than water, such as dimethyl sulfoxide,[12] alcohols,[13] ethers,[14,15] or chelating agents ethylenediaminetetraacetate[16] and ethylene glycol.[17] Specifically, the addition of these small molecules can partially or fully displace water in the first solvation shell or disrupt the water network through the formation of additional hydrogen bonds, which in turn leads to the preferential reduction of solvated organic molecules. Recently, the addition of acetonitrile has been proposed to improve the electrochemical properties and durability of $ZnSO_4$-based batteries.[18] Acetonitrile is a very inexpensive additive and is highly miscible with water, which makes it a good candidate for aqueous ZIB technologies. However, acetonitrile does not dissolve $ZnSO_4$, making it an antisolvent in this system. Given that the exact role of antisolvents in batteries is generally not clear,[13,19,20] uncovering their role in improved electrochemical performance may help the design of stable and durable batteries. Furthermore, there are a growing number of reports on additives in which claims of improved performance are accepted without sufficient *experimental* evidence for the mechanisms by which these performance improvements are achieved. More comprehensive evaluation procedures are needed that combine computational *and* experimental evaluation of deposition/stripping mechanisms to accelerate progress in battery technologies.

Herein, we present a joint experimental and theoretical investigation to reveal the mechanism behind the improved performance of aqueous Zn batteries upon the addition of acetonitrile as an antisolvent. X-ray adsorption near-edge spectroscopy (XANES), extended X-ray absorption fine structure spectroscopy (EXAFS), X-ray pair distribution function (PDF), and Raman measurements on 1 M $ZnSO_4$ samples with up to 10 vol% acetonitrile all indicate that acetonitrile does not penetrate the first solvation shell of Zn^{2+}, consistent with its antisolvent properties. This finding is also observed in molecular dynamics (MD) simulations. Double-layer capacitance measurements and shell-isolated nanoparticle-enhanced Raman spectroscopy (SHINERS) experiments indicate that, rather than modifying bulk solvation, acetonitrile instead modifies the interfacial chemistry, likely by adsorbing onto the electrode surface, resulting in modified Zn deposition and HER kinetics. Scanning electron microscopy (SEM) imaging and elemental analysis (energy-dispersive spectroscopy, EDS) of copper working electrodes extracted after half-cell cycling experiments further reveal that acetonitrile impacts the evolution of deposit morphology over subsequent cycles by modifying zinc nucleation and slowing the ZHS formation rate. The difference in half-cell cycling performance was assessed using cumulative Coulombic efficiency (CCE), which showed that addition of any amount of acetonitrile resulted in decreased losses of active Zn from cycle to cycle. Overall, this study provides fundamental knowledge on the control of interfacial processes by antisolvents and offers practical strategies for improvements in the efficiency and durability of ZIB technologies.

Zn-Ion Bulk Solvation. Changes in the bulk solvation structure of Zn^{2+} upon the addition of acetonitrile were probed using electronic and vibrational spectroscopies. As shown in Figure 1a,b, the addition of acetonitrile yields no noticeable changes in the electronic structure of the $[Zn(H_2O)_6]^{2+}$ complex, suggesting that acetonitrile does not displace water in the first coordination shell, regardless of concentration (more X-ray and Raman data can be found in sections 2 and 3 in the Supporting Information).

The bulk solvation of Zn^{2+} in acetonitrile/water mixtures was also probed by using MD simulations. Details on the simulations and validation of the methods used are provided in the Supporting Information and Figure S9. The calculated coordination numbers (CNs) of water and acetonitrile surrounding Zn^{2+} are summarized in Figure 1c. Without acetonitrile, each Zn^{2+} is coordinated by an average of 6.0 water molecules. With the increase of acetonitrile up to 10 vol %, the water CN barely decreases to 5.8 and the CN of acetonitrile reaches only ∼0.2. Therefore, Zn^{2+} is mainly coordinated by water, with a low probability of acetonitrile entering the first solvation shell with nitrogen coordinating to Zn^{2+} (see Figures 1c and S11). While the acetonitrile coordination probability increases with increasing acetonitrile composition, it is important to note that the CN remains at a very low value compared to that of water. The proposed solvation structure in the bulk and additional site-to-site radial distribution function calculations are summarized in section 4 in the Supporting Information.

Zn-Ion Interfacial Solvation. Based on the experimental and computational results discussed above, we conclude that acetonitrile does not displace water molecules in the first solvation shell of Zn^{2+} to any significant extent. Thus, it is

https://doi.org/10.1021/acsenergylett.3c02504
ACS Energy Lett. 2024, 9, 201−208

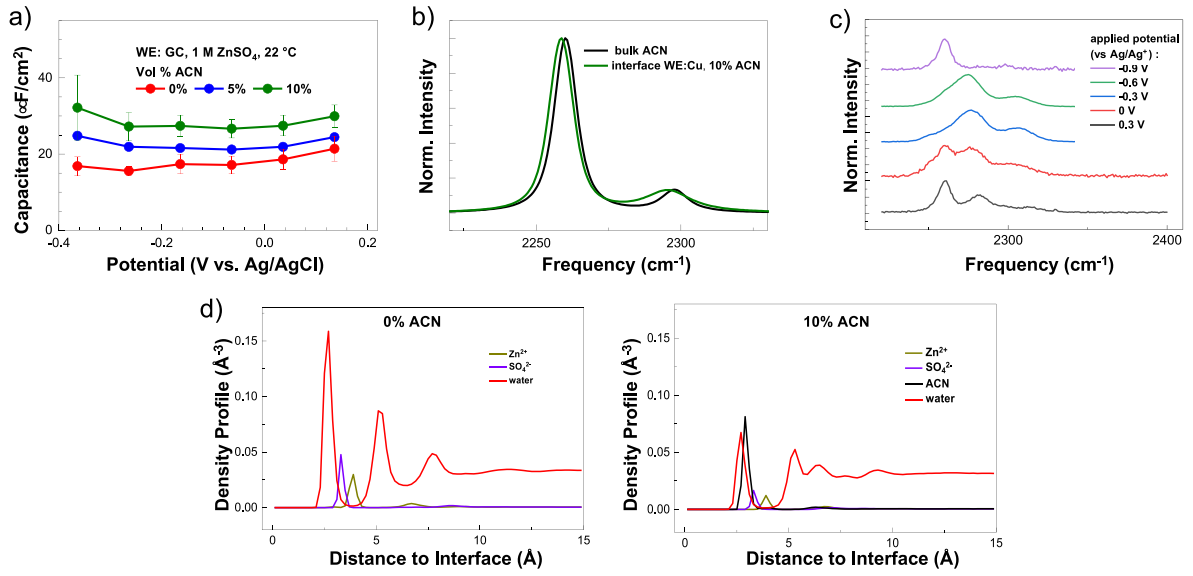

Figure 2. Effect of acetonitrile on interfacial structure: (a) capacitance dependence on the applied potential and acetonitrile content on glassy carbon electrode; (b) acetonitrile C−N band in the bulk and at the interface in SHINERS experiments; (c) acetonitrile C−N band at the interface as a function of applied potential; and (d) calculated number density profiles for 0% and 10% acetonitrile.

likely that the beneficial properties of acetonitrile instead manifest at the electrode−electrolyte interface. The effect of acetonitrile on interfacial solvation structure was probed using cyclic voltammetry (CV) on glassy carbon.[21] Results depicted in Figure 2a indicate that the introduction of acetonitrile disrupts the electrochemical double layer at the electrode interface, given that the apparent double-layer capacitance (C_{dl}) increases from 18 $\mu F/cm^2$ in 0 vol% acetonitrile to 30 $\mu F/cm^2$ in 10 vol% acetonitrile. Similar behavior is also observed for copper working electrodes (Figure S13).

Further insights on the interfacial role of acetonitrile were obtained using SHINERS,[22,23] which is an *in situ*, surface-enhanced Raman scattering technique that utilizes silica-coated gold nanoparticles to achieve the interface-specific surface plasmon resonance effect while preventing participation of the Au core in the electrochemical measurement (Scheme S1). First, we compare the effect of acetonitrile on the interface chemistry of the copper electrode using SO_4^{2-} bands as a proxy for the solvation structure of Zn^{2+}. As shown in Figure S14, the addition of acetonitrile yields no noticeable changes in the SO_4^{2-} band at 980 cm^{-1}, indicating that, at open circuit, acetonitrile likely does not disturb the first solvation shell of Zn^{2+} or SO_4^{2-}, even at the interface. In contrast to the SO_4^{-} modes, SHINERS measurements at open circuit reveal a modest red shift for both acetonitrile bands and a slight broadening of the 2300 cm^{-1} band (Figure 2b and Figure S15). Furthermore, the extent of this red shift appears to be surface dependent and may indicate different affinities toward acetonitrile (Figure S16). The observed behavior suggests two possible scenarios: surface binding of acetonitrile or a significant alteration in the surface dielectric properties due to the presence of acetonitrile near the interface.

Additional insights into the acetonitrile participation were obtained by applying varying potentials on the copper working electrode (Figure 2c). When a potential of 0.3 V (vs Ag/Ag^+) is applied to the electrode, an intermediate shoulder emerges for the C−N stretching mode (Figure 2c). Upon applying more negative potentials (0 to −0.6 V vs Ag/Ag^+), the shoulder becomes more pronounced before it diminishes at −0.9 V, which we assign to the plating regime. This new shoulder feature could be due to the interaction of adsorbing electroactive species with acetonitrile, or it could be an indication of the surface adsorption of acetonitrile. Given that we observe no peak changes in the SO_4^{2-} bands (Figure S17), we speculate that acetonitrile is likely specifically adsorbed on copper. We note that glassy carbon does not show intermediate shoulders in the same potential range, further suggesting that specific adsorption takes place on the Cu-metal electrode (Figure S18). Taken together, the capacitance and SHINERS experiments provide clear evidence that acetonitrile preferentially segregates to the electrode−electrolyte interface and likely specifically adsorbs to metal electrode surfaces at applied potential biases.

The role of acetonitrile at the electrode interface was also studied by MD simulation (details on interfacial simulations can be found in section 7 in the Supporting Information).[24] Figure 2e provides the density profiles of each species as a function of distance from the copper surface. As expected, water plays a dominant role on the surface when acetonitrile is absent, as indicated by the high peak at the distance of 2.7 Å. However, once acetonitrile is added to the solution, it tends to replace water near electrodes. At 10% acetonitrile (90% water), the acetonitrile peak height at the same distance already surpasses that of water, suggesting a more preferential distribution of acetonitrile at the copper surface than that of water. Snapshots of the liquid structure at the simulated copper surface at 0% and 10% acetonitrile are shown in Figure S20. The preferred distribution of acetonitrile at the copper surface can also be seen in the normalized density profile shown in Figure S21, which is relative to the number density of each species in the middle of the simulation box (bulk density). In all solutions, acetonitrile has a higher normalized number density at the surface than all other species in the solution, suggesting their favorable adsorption to the copper surface. Furthermore, the site-to-site CNs of the acetonitrile N atom and water O atom for the Zn^{2+} ions located in the first layer to the copper surface were calculated. The result shows that the CN of the N atom remains low at all acetonitrile

https://doi.org/10.1021/acsenergylett.3c02504
ACS Energy Lett. 2024, 9, 201−208

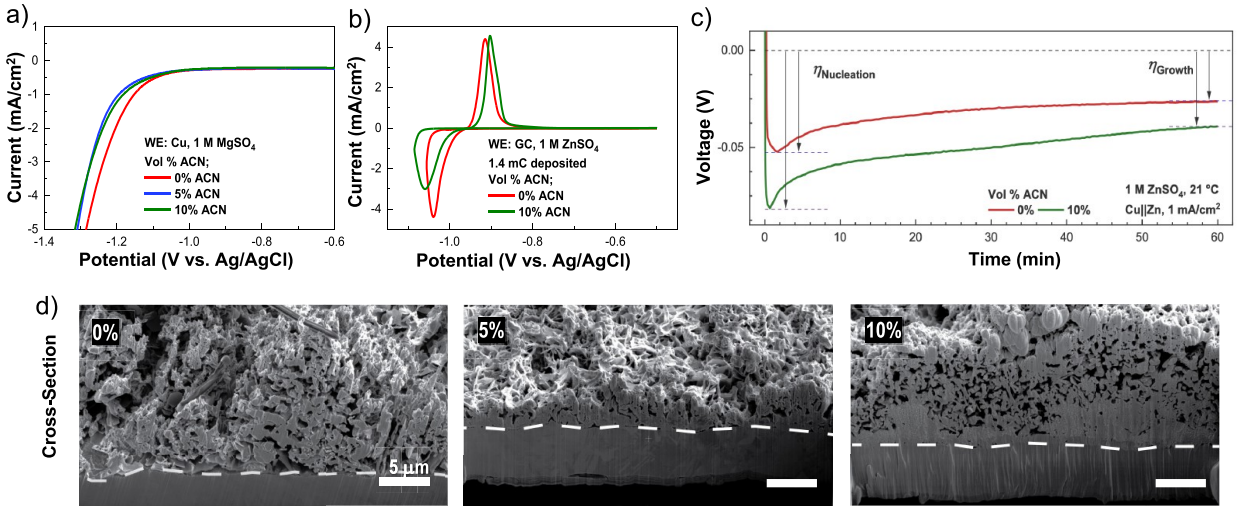

Figure 3. Effect of acetonitrile on the surface electrochemistry: (a) cyclic voltammetry of 1 M $ZnSO_4$ using glassy carbon electrode in the presence and absence of acetonitrile; (b) negative linear sweep of 1 M $MgSO_4$ as a function of added acetonitrile; and (c) comparison of the initial plating step in Cu||Zn coin cells with 1 M $ZnSO_4$ electrolyte with 0 and 10 vol% acetonitrile added. Nucleation and growth overpotentials are defined in the graph. (d) SEM images of zinc deposits on select copper electrodes after plating, stripping, and plating 1 mA/cm^2, 1 mAh/cm^2 zinc at 0, 5, and 10 vol% acetonitrile. White dashed lines separate the Cu substrate from deposited Zn, as determined using EDS in Figure S25.

concentrations (highest 0.33 for 10% acetonitrile). On the other hand, the CN for water remains close to 6 in all studied systems. The CN for acetonitrile to SO_4^{2-} was found to be even lower (highest of 0.12 for 10% acetonitrile), whereas the water CN surrounding a SO_4^{2-} is always around 12 (Figure S12). These characteristics are consistent with experimental observations and further indicate that acetonitrile disrupts the electrochemical double layer at the electrode interface by replacing water with Zn^{2+} and SO_4^{2-}.

Implications on the Surface Electrochemistry. The presence of acetonitrile at the electrode surface will have implications for both zinc metal plating and stripping, as well as parasitic reactions during cell operation. Figure 3a shows CVs of 1 M $ZnSO_4$ in the presence and absence of acetonitrile, depicting the deposition/stripping processes on glassy carbon.[21] Noticeably, an ∼50 mV increase in the onset overpotential is consistently observed in the presence of acetonitrile. The origin of this increase could be attributed to the displacement of electroactive Zn^{2+} from the electrode surface by adsorbed acetonitrile, since more energy is required to desorb acetonitrile and plate zinc.[25,26] The acetonitrile is likely always present on the substrate and plated zinc electrode surface, given that both plating and stripping overpotentials (as measured at 1 mA/cm^2) shift to ∼20 mV higher overpotentials.

The presence of acetonitrile at the electrode surface and disruption of typical water−ion structures also have implications for the HER, a critical challenge in neutral-pH zinc metal batteries that lowers CE during zinc plating and at open circuit through spontaneous corrosion of zinc metal. Figure 3b shows linear sweep voltammetry focusing on the onset of HER on Cu electrodes in 1 M $MgSO_4$. As shown, the addition of acetonitrile shifts the apparent onset of HER to more negative potentials, the ideal case for preventing HER during zinc plating. However, the exact amount of acetonitrile does not matter; i.e., adding more acetonitrile does not increase the overpotential further. Similar results were observed for 1 M Na_2SO_4 (Figure S22).

Implications on Zn-Ion Battery Performance. To isolate the contribution of acetonitrile to the zinc plating and stripping, we used half-cells with copper working electrodes and zinc anodes. Figure 3c shows the onset of zinc plating at 0% acetonitrile and 10% acetonitrile on the first cycle of Cu||Zn half-cells under galvanostatic cycling at 1 mA/cm^2. The nucleation overpotential in the first step, which reflects the overpotential required to deposit zinc onto the fresh copper surface,[27] is significantly higher with larger amounts of acetonitrile compared to the pure water condition, analogous to the CV results in Figure 3a. The effective growth overpotential[28] also increases with 10% acetonitrile. Similarly, the effective stripping potential is, on average, ∼15 mV higher (Figure S23), consistent with the observations in CV experiments shown in Figure 3a.

To determine the physical impact on the early stage of zinc plating, SEM was performed on the copper anode of coin cells after plating, stripping, and plating once more at 1 mA/cm^2, 1 mAh/cm^2 (Figures 3d and S24). Qualitatively, the metallic zinc deposits without any acetonitrile are larger than those with acetonitrile (Figure S24). It appears that increasing the nucleation overpotential with high acetonitrile content decreases the size of the initial zinc nuclei, leading to smaller zinc deposits, consistent with previously reported studies[29,30] and expectations from simple spherical nucleation models.[27] The morphologies of the metallic Zn deposits are highly porous, as can be seen in the cross-sectional view from focused ion beam (FIB) milling in Figure 3d. In the areas sampled, the metallic Zn deposits can grow an initial dense layer closest to the surface of the Cu electrode but then grow to be porous, with "mossy" structures, above the immediate surface layer. The height of the metallic Zn deposits highly varies, e.g., up to 15 μm in the sample without acetonitrile in the area sampled. It is important to note that, although the areas sampled are small (∼30 μm) due to the nature of Ga-ion beams used in the FIB, areas that are representative of the surface morphologies were selected.

https://doi.org/10.1021/acsenergylett.3c02504
ACS Energy Lett. 2024, 9, 201−208

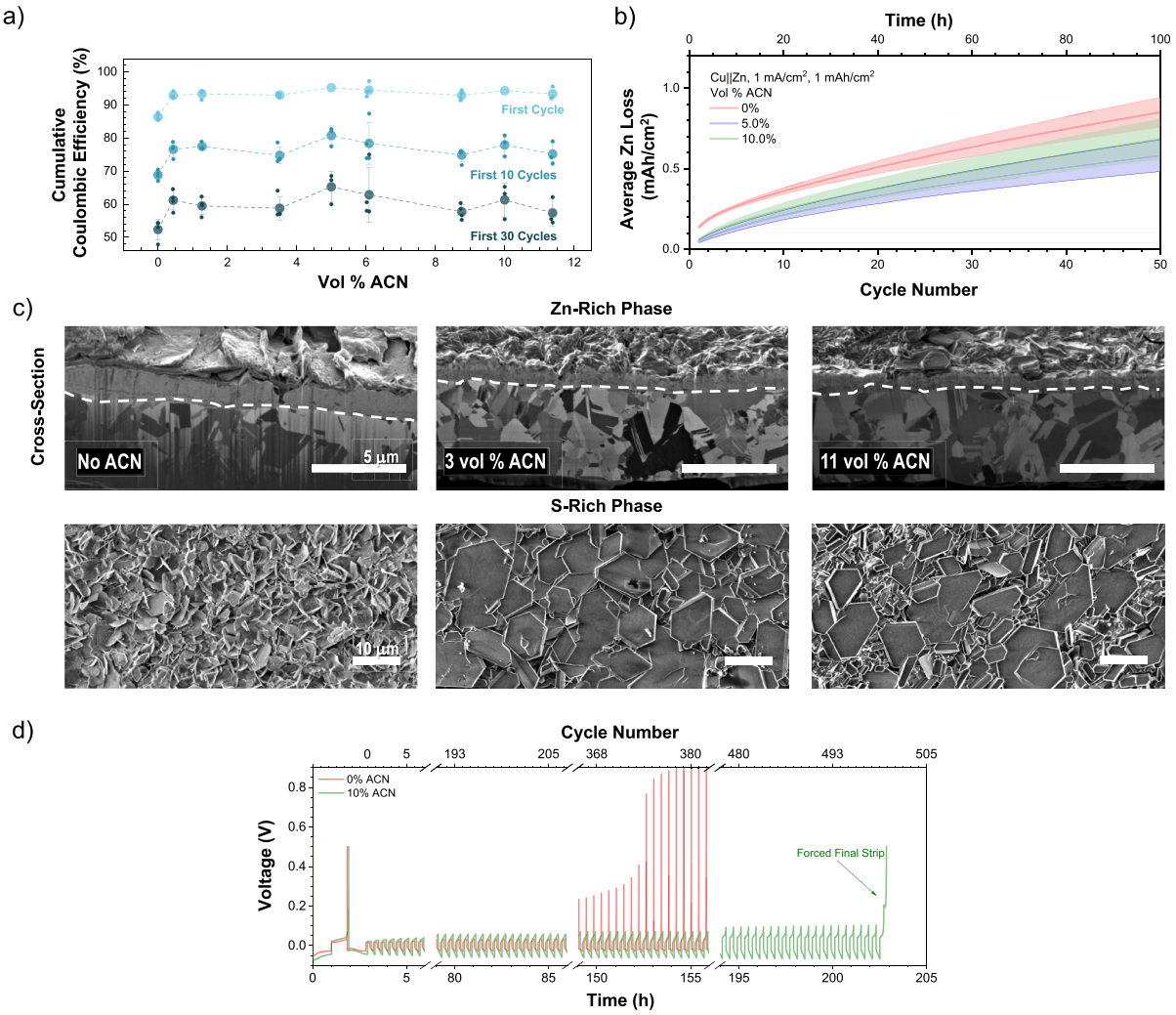

Figure 4. Coulombic efficiency and long-term morphology: (a) Cumulative CEs of cells over cycle lifetime, integrated over the first 1, 10, and 30 cycles. Small dots represent individual cells, while larger points and error bars represent the average and standard deviation of at least three different cells. (b) Total charge loss over time for Cu||Zn half-cells at 100% DOD. Solid lines are averages for four cells; shaded areas represent standard deviation. (c) SEM images of zinc deposits and ZHS formation on select copper electrodes after 100 cycles and one additional plating step at 1 mA/cm², 1 mAh/cm² for 0, 3, and 11 vol% acetonitrile. White dashed lines separate Cu substrate from deposited Zn, as determined using EDS in Figure S27. (d) Cycling profiles of Cu||Zn half-cells with 0 and 10 vol% acetonitrile at 1 mA/cm² at 20% DOD, with 1 mAh/cm² preconditioning and 1 mAh/cm² plated reservoir.

To access the long-term effects of acetonitrile on the zinc plating and stripping as previous works have done, we performed continuous plating and stripping to 100% depth of discharge (DOD) at 1 mA/cm², 1 mAh/cm² on the same cells from Figure 3c,d. The efficiency of these processes was analyzed using "cumulative" or "compounded" Coulombic efficiency (CCE), which is an emerging quantity especially in the lithium metal anode field.[31−33] This is a more accurate measure of charge loss in the cell since it integrates the efficiency over every cycle, not just cycle-to-cycle, and is defined as

$$\text{Cumulative CE} = 100 \times \prod_{1}^{n} \frac{Q_{\text{strip},n}}{Q_{\text{plate},n}} \quad (1)$$

where n is the number of cycles and $Q_{\text{strip},n}$ and $Q_{\text{plate},n}$ are the stripped and plated charges at each nth cycle, respectively. This analysis was applied to multiple cells and is plotted in Figure 4a for the first 10 and first 30 cycles. In the first cycle, 0 vol% acetonitrile shows 86% CE, while any amount of acetonitrile increases the CE to the range of 92−96% CE. With more cycles, this trend holds, with pure water always showing a lower CCE than acetonitrile. Importantly, there is little to no statistical difference in the CCE with increasing acetonitrile concentration, with more cell-to-cell variation within a given acetonitrile concentration than variation between concentrations. This indicates that any amount of acetonitrile will improve CE relative to pure water as the solvent.[34] Also of note is that the CCE drops to below 60% before even 50 cycles under these conditions, indicating that further optimization of the electrolyte, separator, electrode, and charge−discharge parameters is required to establish a reliable zinc electrode at scale. These results highlight the impracticality of 100% DOD testing protocols but also the importance of using CCE instead of CE alone in characterizing battery performance, as we eventually observe 99%+ individual cycle efficiencies for all samples using the conventional protocol (Figure S32).

https://doi.org/10.1021/acsenergylett.3c02504
ACS Energy Lett. 2024, 9, 201−208

The morphologies of Zn deposits after 100 cycles (Figures 4c and S26) share some characteristics with the samples after one cycle (Figures 3d and S24). The Zn deposits grow to form a dense layer first, then a "mossy" structures on the surface, possibly as a result of Zn deposits growing into the separator,[35] as can be seen in the top row of images in Figure S26. In contrast, the cross sections are dense and do not show porosities in the areas sampled, different from the samples after 1 cycle. The thicknesses of the Zn deposits are also smaller compared to those in the samples with 100 cycles,[36] as shown in Figure 4c. The depths of the Zn deposits are measured to be around 2 μm for the sample with 0%, 1 μm for 3%, and 1.1 μm for 11% acetonitrile concentrations. The slightly thicker Zn deposits observed for 0% acetonitrile may indicate a film swelling, likely due to more HER. Different areas on each electrode, however, can show different morphologies. The regions selected in Figure 4c are representative of areas with Zn deposits, although different morphologies can exist at the edges of these regions (as shown in Figure S28).

It is interesting to note that ZHS formation was observed in all samples after 100 cycles but with morphologies that are distinct from metallic Zn deposits (Figure 4c, bottom panel). The ZHS formations appear to have stronger tendencies of faceting in acetonitrile-containing samples, as reflected in the highly geometric shapes; the EDS maps show a faceted grain for 3 vol% acetonitrile that is clearly S-rich compared to the adjacent Zn deposits, evidence that the faceted grains are indeed ZHS crystals (Figure S29). Both 3 and 11 vol% acetonitrile yield significantly bigger crystals than samples without acetonitrile, which can be correlated to the fact that acetonitrile dictates ZHS morphology by lowering HER rates (Figure 3b). Apart from different morphologies, the EDS data on the same areas show overall less sulfur content in 3 and 11 vol% acetonitrile, which is consistent with inhibited HER kinetics (Figures S30 and S31). These electrodes with 3 and 11 vol% acetonitrile show the same trend as 5 and 10 vol% acetonitrile, showing again that small changes in acetonitrile in this concentration regime do not significantly impact Zn electrochemistry.[32] The highly oriented ZHS crystals and lower overall ZHS content are likely the reason for the improved CCE values in Figure 4a, given that a recent study showed that this ZHS morphology provides a more stable solid–electrolyte interface.[5]

To probe the long-term stability of the zinc anode, we performed continuous plating and stripping at 1 mA/cm^2 with 20% DOD after plating 1 mAh/cm^2, with CE calculated using the Adams method.[37,38] As shown in Figures 4d and S33a, cells utilizing 0% acetonitrile deplete the Zn reservoir after 150 h (<375 cycles) with CE = 99.27 ± 0.06%. Remarkably, cells containing 10% acetonitrile cycled at least 425 cycles, and two out of three cells cycled up to 500 cycles before being intentionally stopped (Figure S33b) with CE = 99.61 ± 0.24%. These CEs correspond to 3.0 ± 0.3 and 2.1 ± 0.2 μAh/cm^2 zinc loss per cycle for 0% and 10% acetonitrile, respectively, further highlighting the improvement in long-term anode health with this solvent additive.

In conclusion, acetonitrile was studied as an additive for aqueous Zn anode batteries. Acetonitrile—a widely available, low-cost, and water-miscible liquid—was shown to act as an antisolvent due to its inability to dissolve $ZnSO_4$, a property that is further corroborated by the lack of acetonitrile in the first Zn^{2+} solvation shell. Instead, acetonitrile is shown to modify the electrode–electrolyte interface on multiple electrode surfaces by adsorbing on the electrode and displacing water and $ZnSO_4$ from the electrode surface. As a result, significant changes in the surface (electro)chemistry were observed, with modified overpotentials for plating/stripping processes and the HER. These surface alterations contribute to different morphologies of zinc metal and ZHS deposits, which improve the overall performance of half-cells with acetonitrile. Future studies should focus on the extent to which electrode–antisolvent interactions can be leveraged to modify interfacial (electro)chemistry and direct the preferential growth of zinc deposits while fully suppressing ZHS formation. Overall, this study offers guiding principles for a detailed and systematic analysis of antisolvents, and additives in general, in aqueous zinc batteries and beyond. We hope that strategies and techniques discussed here will help bridge the gap in understanding between electrolyte design and battery performance.

■ ASSOCIATED CONTENT

Supporting Information

The Supporting Information is available free of charge at https://pubs.acs.org/doi/10.1021/acsenergylett.3c02504.

Detailed experimental and computational sections; PDF data fits; more Raman spectroscopy data of the bulk and interface; simulation data of the bulk and interface; detailed SEM and EDS analyses; long-term cycling performance (PDF)

■ AUTHOR INFORMATION

Corresponding Author

Sanja Tepavcevic − *Joint Center for Energy Storage Research and Material Science Division, Argonne National Laboratory, Lemont, Illinois 60439, United States;* orcid.org/0000-0003-0151-8832; Email: sanja@anl.gov

Authors

Stefan Ilic − *Joint Center for Energy Storage Research and Material Science Division, Argonne National Laboratory, Lemont, Illinois 60439, United States;* orcid.org/0000-0002-6305-4001

Michael J. Counihan − *Joint Center for Energy Storage Research and Material Science Division, Argonne National Laboratory, Lemont, Illinois 60439, United States*

Sydney N. Lavan − *Joint Center for Energy Storage Research and Material Science Division, Argonne National Laboratory, Lemont, Illinois 60439, United States*

Yingjie Yang − *Department of Physics, University of Illinois at Chicago, Chicago, Illinois 60607, United States;* orcid.org/0000-0002-1898-8171

Yinke Jiang − *Joint Center for Energy Storage Research, Argonne National Laboratory, Lemont, Illinois 60439, United States; Department of Chemical and Biomolecular Engineering, University of Notre Dame, Notre Dame, Indiana 46556, United States*

Diwash Dhakal − *Joint Center for Energy Storage Research, Argonne National Laboratory, Lemont, Illinois 60439, United States; Department of Materials Science and Engineering, University of Washington, Washington 98195, United States*

Julian Mars − *Joint Center for Energy Storage Research, Argonne National Laboratory, Lemont, Illinois 60439, United States; Department of Chemical and Biological*

https://doi.org/10.1021/acsenergylett.3c02504
ACS Energy Lett. 2024, 9, 201−208

Engineering, University of Colorado Boulder, Boulder, Colorado 80309, United States

Emma N. Antonio − *Joint Center for Energy Storage Research, Argonne National Laboratory, Lemont, Illinois 60439, United States; Department of Chemical and Biological Engineering, University of Colorado Boulder, Boulder, Colorado 80309, United States*

Luis Kitsu Iglesias − *Department of Chemical and Biological Engineering, University of Colorado Boulder, Boulder, Colorado 80309, United States;* orcid.org/0000-0002-9292-4416

Timothy T. Fister − *Joint Center for Energy Storage Research and Chemical Sciences and Engineering Division, Argonne National Laboratory, Lemont, Illinois 60439, United States;* orcid.org/0000-0001-6537-6170

Yong Zhang − *Joint Center for Energy Storage Research, Argonne National Laboratory, Lemont, Illinois 60439, United States; Department of Chemical and Biomolecular Engineering, University of Notre Dame, Notre Dame, Indiana 46556, United States;* orcid.org/0000-0003-3988-5961

Edward J. Maginn − *Joint Center for Energy Storage Research, Argonne National Laboratory, Lemont, Illinois 60439, United States; Department of Chemical and Biomolecular Engineering, University of Notre Dame, Notre Dame, Indiana 46556, United States;* orcid.org/0000-0002-6309-1347

Michael F. Toney − *Joint Center for Energy Storage Research, Argonne National Laboratory, Lemont, Illinois 60439, United States; Department of Chemical and Biological Engineering, University of Colorado Boulder, Boulder, Colorado 80309, United States;* orcid.org/0000-0002-7513-1166

Robert F. Klie − *Joint Center for Energy Storage Research, Argonne National Laboratory, Lemont, Illinois 60439, United States; Department of Physics, University of Illinois at Chicago, Chicago, Illinois 60607, United States;* orcid.org/0000-0003-4773-6667

Justin G. Connell − *Joint Center for Energy Storage Research and Material Science Division, Argonne National Laboratory, Lemont, Illinois 60439, United States;* orcid.org/0000-0002-2979-2131

Complete contact information is available at: https://pubs.acs.org/10.1021/acsenergylett.3c02504

Notes

The authors declare no competing financial interest.

■ ACKNOWLEDGMENTS

This work was supported as part of the Joint Center for Energy Storage Research (JCESR), an Energy Innovation Hub funded by the U.S. Department of Energy (DOE), Office of Science, Basic Energy Sciences. This research used resources of the Advanced Photon Source, a U.S. DOE Office of Science user facility at Argonne National Laboratory. Electrochemical measurements and Raman spectroscopy were performed at the Electrochemical Discovery Laboratory, a JCESR facility at Argonne National Laboratory. This work made use of the ThermoFisher Helios 5CX (cryo)FIB-SEM instrument in the Electron Microscopy Core of UIC's Research Resources Center, which received support from UIC, Northwestern University, and ARO (W911NF2110052). Y.J., Y.Z., and E.J.M. thank the Center for Research Computing (CRC) at the University of Notre Dame for providing computational resources.

■ REFERENCES

(1) Trahey, L.; Brushett, F. R.; Balsara, N. P.; Ceder, G.; Cheng, L.; Chiang, Y.-M.; Hahn, N. T.; Ingram, B. J.; Minteer, S. D.; Moore, J. S.; Mueller, K. T.; Nazar, L. F.; Persson, K. A.; Siegel, D. J.; Xu, K.; Zavadil, K. R.; Srinivasan, V.; Crabtree, G. W. Energy Storage Emerging: A Perspective from the Joint Center for Energy Storage Research. *Proc. Natl. Acad. Sci. U.S.A.* **2020**, *117* (23), 12550−12557.

(2) Lu, W.; Zhang, C.; Zhang, H.; Li, X. Anode for Zinc-Based Batteries: Challenges, Strategies, and Prospects. *ACS Energy Lett.* **2021**, *6* (8), 2765−2785.

(3) Liu, C.; Xie, X.; Lu, B.; Zhou, J.; Liang, S. Electrolyte Strategies toward Better Zinc-Ion Batteries. *ACS Energy Lett.* **2021**, *6* (3), 1015−1033.

(4) Wan, F.; Zhou, X.; Lu, Y.; Niu, Z.; Chen, J. Energy Storage Chemistry in Aqueous Zinc Metal Batteries. *ACS Energy Lett.* **2020**, *5* (11), 3569−3590.

(5) Wang, J.; Zhang, B.; Cai, Z.; Zhan, R.; Wang, W.; Fu, L.; Wan, M.; Xiao, R.; Ou, Y.; Wang, L.; Jiang, J.; Seh, Z. W.; Li, H.; Sun, Y. Stable Interphase Chemistry of Textured Zn Anode for Rechargeable Aqueous Batteries. *Sci. Bull. (Beijing)* **2022**, *67* (7), 716−724.

(6) Yuan, W.; Ma, G.; Nie, X.; Wang, Y.; Di, S.; Wang, L.; Wang, J.; Shen, S.; Zhang, N. In-Situ Construction of a Hydroxide-Based Solid Electrolyte Interphase for Robust Zinc Anodes. *Chem. Eng. J.* **2022**, *431*, No. 134076.

(7) Suo, L.; Borodin, O.; Gao, T.; Olguin, M.; Ho, J.; Fan, X.; Luo, C.; Wang, C.; Xu, K. Water-in-Salt" Electrolyte Enables High-Voltage Aqueous Lithium-Ion Chemistries. *Science (1979)* **2015**, *350* (6263), 938−943.

(8) Wang, F.; Borodin, O.; Gao, T.; Fan, X.; Sun, W.; Han, F.; Faraone, A.; Dura, J. A.; Xu, K.; Wang, C. Highly Reversible Zinc Metal Anode for Aqueous Batteries. *Nat. Mater.* **2018**, *17* (6), 543−549.

(9) Leonard, D. P.; Wei, Z.; Chen, G.; Du, F.; Ji, X. Water-in-Salt Electrolyte for Potassium-Ion Batteries. *ACS Energy Lett.* **2018**, *3* (2), 373−374.

(10) Jin, T.; Ji, X.; Wang, P.; Zhu, K.; Zhang, J.; Cao, L.; Chen, L.; Cui, C.; Deng, T.; Liu, S.; Piao, N.; Liu, Y.; Shen, C.; Xie, K.; Jiao, L.; Wang, C. High-Energy Aqueous Sodium-Ion Batteries. *Angew. Chem., Int. Ed.* **2021**, *60* (21), 11943−11948.

(11) Droguet, L.; Grimaud, A.; Fontaine, O.; Tarascon, J. Water-in-Salt Electrolyte (WiSE) for Aqueous Batteries: A Long Way to Practicality. *Adv. Energy Mater.* **2020**, *10* (43), No. 2002440.

(12) Cao, L.; Li, D.; Hu, E.; Xu, J.; Deng, T.; Ma, L.; Wang, Y.; Yang, X.-Q.; Wang, C. Solvation Structure Design for Aqueous Zn Metal Batteries. *J. Am. Chem. Soc.* **2020**, *142* (51), 21404−21409.

(13) Zhu, Y.; Hao, J.; Huang, Y.; Jiao, Y. A New Insight of Anti-Solvent Electrolytes for Aqueous Zinc-Ion Batteries by Molecular Modeling. *Small Struct.* **2023**, *4* (4), 270 DOI: 10.1002/sstr.202200270.

(14) He, W.; Ren, Y.; Lamsal, B. S.; Pokharel, J.; Zhang, K.; Kharel, P.; Wu, J. J.; Xian, X.; Cao, Y.; Zhou, Y. Decreasing Water Activity Using the Tetrahydrofuran Electrolyte Additive for Highly Reversible Aqueous Zinc Metal Batteries. *ACS Appl. Mater. Interfaces* **2023**, *15* (5), 6647−6656.

(15) Wei, T.; Ren, Y.; Wang, Y.; Mo, L.; Li, Z.; Zhang, H.; Hu, L.; Cao, G. Addition of Dioxane in Electrolyte Promotes (002)-Textured Zinc Growth and Suppressed Side Reactions in Zinc-Ion Batteries. *ACS Nano* **2023**, *17* (4), 3765−3775.

(16) Meng, R.; Li, H.; Lu, Z.; Zhang, C.; Wang, Z.; Liu, Y.; Wang, W.; Ling, G.; Kang, F.; Yang, Q. Tuning Zn-Ion Solvation Chemistry with Chelating Ligands toward Stable Aqueous Zn Anodes. *Adv. Mater.* **2022**, *34* (37), No. 2200677.

(17) Verma, V.; Chan, R. M.; Jia Yang, L.; Kumar, S.; Sattayaporn, S.; Chua, R.; Cai, Y.; Kidkhunthod, P.; Manalastas, W.; Srinivasan, M. Chelating Ligands as Electrolyte Solvent for Rechargeable Zinc-Ion Batteries. *Chem. Mater.* **2021**, *33* (4), 1330−1340.

(18) Hou, Z.; Tan, H.; Gao, Y.; Li, M.; Lu, Z.; Zhang, B. Tailoring Desolvation Kinetics Enables Stable Zinc Metal Anodes. *J. Mater. Chem. A Mater.* **2020**, *8* (37), 19367−19374.
(19) Wu, Y.; Wang, A.; Hu, Q.; Liang, H.; Xu, H.; Wang, L.; He, X. Significance of Antisolvents on Solvation Structures Enhancing Interfacial Chemistry in Localized High-Concentration Electrolytes. *ACS Cent Sci.* **2022**, *8* (9), 1290−1298.
(20) Wen, J.; Fu, H.; Zhang, D.; Ma, X.; Wu, L.; Fan, L.; Yu, X.; Zhou, J.; Lu, B. Nonfluorinated Antisolvents for Ultrastable Potassium-Ion Batteries. *ACS Nano* **2023**, *17*, 16135.
(21) Glassy carbon was used primarily to probe a wider potential range without side reactions relative to metals such as copper and zinc (e.g., oxide chemistry, oxygen reduction, and alloying).
(22) Li, J. F.; Huang, Y. F.; Ding, Y.; Yang, Z. L.; Li, S. B.; Zhou, X. S.; Fan, F. R.; Zhang, W.; Zhou, Z. Y.; Wu, D. Y.; Ren, B.; Wang, Z. L.; Tian, Z. Q. Shell-Isolated Nanoparticle-Enhanced Raman Spectroscopy. *Nature* **2010**, *464* (7287), 392−395.
(23) Wu, D.-Y.; Li, J.-F.; Ren, B.; Tian, Z.-Q. Electrochemical Surface-Enhanced Raman Spectroscopy of Nanostructures. *Chem. Soc. Rev.* **2008**, *37* (5), 1025.
(24) The results with zero partial charges on the Cu atoms are reported here. Non-zero partial charge simulations were also carried out, and similar trends were found.
(25) Huang, C.; Zhao, X.; Hao, Y.; Yang, Y.; Qian, Y.; Chang, G.; Zhang, Y.; Tang, Q.; Hu, A.; Chen, X. Selection Criteria for Electrical Double Layer Structure Regulators Enabling Stable Zn Metal Anodes. *Energy Environ. Sci.* **2023**, *16* (4), 1721−1731.
(26) Xiao, P.; Wu, Y.; Fu, J.; Liang, J.; Zhao, Y.; Ma, Y.; Zhai, T.; Li, H. Enabling High-Rate and High-Areal-Capacity Zn Deposition via an Interfacial Preferentially Adsorbed Molecular Layer. *ACS Energy Lett.* **2023**, *8* (1), 31−39.
(27) Yu, X.; Li, Z.; Wu, X.; Zhang, H.; Zhao, Q.; Liang, H.; Wang, H.; Chao, D.; Wang, F.; Qiao, Y.; Zhou, H.; Sun, S.-G. Ten Concerns of Zn Metal Anode for Rechargeable Aqueous Zinc Batteries. *Joule* **2023**, *7* (6), 1145−1175.
(28) The effective growth overpotential is defined here as the most positive potential during plating and is reflective of the overpotential required to continually deposit zinc on the already plated zinc metal.
(29) Liu, H.; Zhang, Y.; Wang, C.; Glazer, J. N.; Shan, Z.; Liu, N. Understanding and Controlling the Nucleation and Growth of Zn Electrodeposits for Aqueous Zinc-Ion Batteries. *ACS Appl. Mater. Interfaces* **2021**, *13* (28), 32930−32936.
(30) Kim, M.; Lee, J.; Kim, Y.; Park, Y.; Kim, H.; Choi, J. W. Surface Overpotential as a Key Metric for the Discharge−Charge Reversibility of Aqueous Zinc-Ion Batteries. *J. Am. Chem. Soc.* **2023**, *145*, 15776.
(31) Schulze, M. C.; Neale, N. R. Half-Cell Cumulative Efficiency Forecasts Full-Cell Capacity Retention in Lithium-Ion Batteries. *ACS Energy Lett.* **2021**, *6* (3), 1082−1086.
(32) Oyakhire, S. T.; Zhang, W.; Yu, Z.; Holmes, S. E.; Sayavong, P.; Kim, S. C.; Boyle, D. T.; Kim, M. S.; Zhang, Z.; Cui, Y.; Bent, S. F. Correlating the Formation Protocols of Solid Electrolyte Interphases with Practical Performance Metrics in Lithium Metal Batteries. *ACS Energy Lett.* **2023**, *8* (1), 869−877.
(33) Bassett, K. L.; Small, K. A.; Long, D. M.; Merrill, L. C.; Warren, B.; Harrison, K. L. Interfacial Pressure Improves Calendar Aging of Lithium Metal Anodes. *Front. Batter. Electrochem.* **2023**, *2*, 1292639 DOI: 10.3389/fbael.2023.1292639.
(34) The amount needed to form a monolayer of acetonitrile ($\sim 3 \times 10^{-8}$ cm^2) is well beyond of those used in experiments, assuming that all acetonitrile adsorbs onto the electrode.
(35) Zhang, Y.; Yang, G.; Lehmann, M. L.; Wu, C.; Zhao, L.; Saito, T.; Liang, Y.; Nanda, J.; Yao, Y. Separator Effect on Zinc Electrodeposition Behavior and Its Implication for Zinc Battery Lifetime. *Nano Lett.* **2021**, *21* (24), 10446−10452.
(36) The boundaries of the interfaces of Zn and Cu are identified with EDS mapping, as shown in Figure S27.
(37) Adams, B. D.; Zheng, J.; Ren, X.; Xu, W.; Zhang, J. Accurate Determination of Coulombic Efficiency for Lithium Metal Anodes and Lithium Metal Batteries. *Adv. Energy Mater.* **2018**, *8* (7), 2097 DOI: 10.1002/aenm.201702097.
(38) Mohammadi, A.; Djafer, S.; Sayegh, S.; Naylor, A. J.; Bechelany, M.; Younesi, R.; Monconduit, L.; Stievano, L. Assessing Coulombic Efficiency in Lithium Metal Anodes. *Chem. Mater.* **2023**, *35* (6), 2381−2393.

https://doi.org/10.1021/acsenergylett.3c02504
ACS Energy Lett. 2024, 9, 201−208